Microchemical Journal 159 (2020) 105489

Contents lists available at ScienceDirect

Microchemical Journal

journal homepage: www.elsevier.com/locate/microc

Electrochemical sensing of methylmalonic acid based on molecularly imprinted polymer modified with graphene oxide and gold nanoparticles

J.R. Deepa, T.S. Anirudhan*, Gowri Soman, V. Chithra Sekhar

Department of Chemistry, School of Physical and Mathematical Sciences, University of Kerala, Trivandrum695 581, Kariavattom, Kerala, India

ARTICLE INFO

Keywords:
Graphene oxide
Gold nanoparticles
Allyl trimethoxysilane molecular imprinting
Methylmalonic acid
Electrochemical sensing

ABSTRACT

Molecularly imprinted allyl trimethoxysilane –grafted- graphene oxide/gold nano particle co polymerised with -allyl amine (AA) /2-aminoethyl methacrylate hydrochloride (AEMA) polymer (GO/AuNP-g-ATMS-co-AEMA/AA) was synthesised by bulk imprinting method. The synthesised product was tested for sensing and quantifying methylmalonic acid (MMA) in blood samples in selective manner. Electrochemical studies performed with the developed sensor. The effective pH for the response of the sensor material was found to be 7.4. The response time, limit of detection (LOD) and limit of quantification (LOQ) of the electrode was found to be ~2 min, 0.2095 μM and 0.2935 μM respectively. The constructed sensor exhibits great selectivity and is useful for the rapid determination of MMA in human serum. The designed electrode is long lasting, reproducible and no pre-treatment of biological samples required during clinical analysis which makes it advantageous. The feasibility of the developed sensor was ensured by comparing it with the HP GC/MSD method practiced in diagnostic laboratory (correlation coefficient of 0.967). These results clearly indicate that the sensor developed through molecularly imprinting technique is valid for real sample analysis.

1. Introduction

Methylmalonic acid (MMA), produced in living system in very small amounts; which is very decisive for metabolism and energy production. Normal levels of methylmalonic acid are between 0.00 and 0.40 μmol/L. Higher levels of MMA in blood and urine serves as early indicator of VB-12 deficiency in living system [1]. VB-12 deficiency is responsible for lacks in maintenance of nerve sheaths, functions of nerves as well as brain and production of red blood cells. VB-12 acts as a cofactor for two important enzymatic reactions; methyl malonyl CoA (a form of MMA) converted to succinyl coenzyme A in mitochondria and conversion of homocysteine (HC) to methionine. Excess methyl malonyl CoA gets converted to MMA. Low levels of VB-12 increase the levels of MMA in blood and urine [2]. Deficiency of VB-12 leads to stomach lining thinned, which causes a condition called atrophic gastritis, which causes failure to absorb VB-12 leads to pernicious anaemia. Due to lack of intrinsic factor in the stomach enough healthy red blood cells cannot be produced in the living system. Another problem of deficiency of VB-12 is emotionlessness and tickling in the hands and feet. In advanced cases, psychological changes like cognitive damage, misperception and gloominess. This may arise due to nutritional factors, malabsorption and other gastrointestinal causes as well [3]. Cancer patients are also vulnerable to VB-12 deficiency because of poor oral consumption, malabsorption, GI surgeries, medications and enteritis. The risk of developing chemotherapy induced peripheral neuropathy (CIPN) in cancer patients increased due to deficiency of vtaminB-12. Deficiency of VB-12 leads to the increased concentration of MMA through the non-formation of blood cells [4,5]. MMA and Homocysteine are valuable for early detection of mild cases of VB-12 deficiency. Hence the MMA concentration can be used as a maker for the VB-12 level for the effective biological process. VB-12 concentration in blood serum could be analysed by radio immune assay. In addition, MMA is also a good maker for monitoring the success of the treatment [6]. Analysis of MMA is very effective in early diagnosis of possible shortages of VB-12 much sooner than the classical analysis [7]. The variation of amount of MMA in blood can easily confirm the availability of VB-12 for metabolic activity. Determination of the concentration of MMA in blood and urine serves as early indicator of VB-12 deficiency in living system, responsible for lacks in maintenance of nerve sheaths as well as functions of nerves and brain and production of red blood cells .

Electrochemical sensing of MMA concentration in blood serum is one of the reliable methods for determination of VB-12 level in the body. An acceptable method for human VB-12 in terms of accuracy, precision and rapidity is still unavailable [8]. Clinical determination of MMA concentration in blood serum is by the method of gas chromatography which is time consuming and not a cost effective technique.

* Corresponding author.
E-mail address: tsani@rediffmail.com (T.S. Anirudhan).

https://doi.org/10.1016/j.microc.2020.105489
Received 16 March 2020; Received in revised form 30 August 2020; Accepted 30 August 2020
Available online 04 September 2020
0026-265X/ © 2020 Elsevier B.V. All rights reserved.

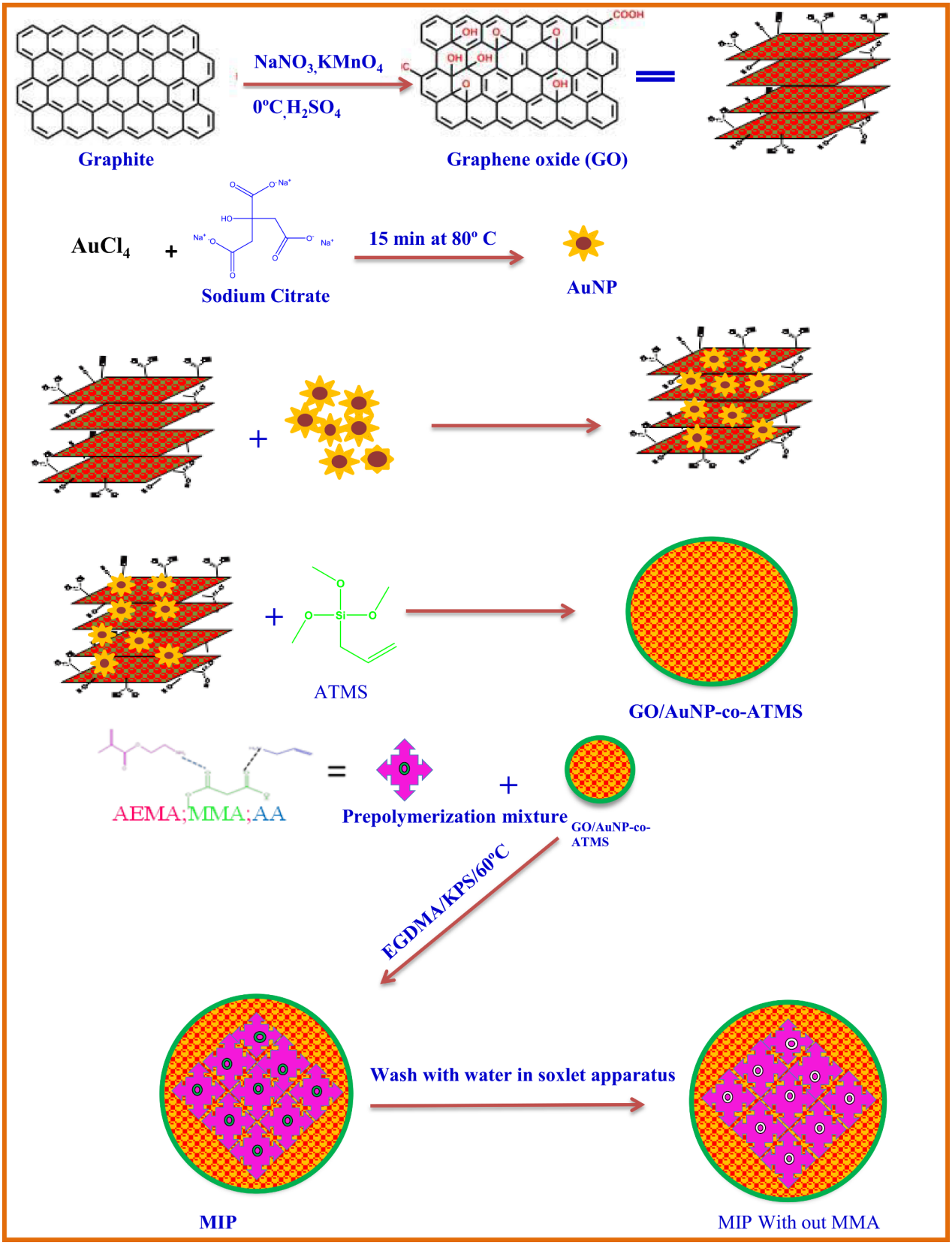

Scheme 1. Scheme for the synthesis of GO/AuNP-co-ATMS-g-AEMA/AA.

Electrochemical method is having various practical advantages like low-cost in instrument, easy and quick operation, and desirable sensitivity and applicable for real-time analysis. This method could subdued the limitations of usual practices like low sensitivity and selectivity, costly set-up and time-consuming. Since the electrochemical sensing of MMA concentration in blood serum is possibly a reliable method for

determination of vitamin B12 as it provides an attractive and effective strategy to analyse the content in biological sample when the biological content directly gets converted to an electrical signal [9]. To the best of our knowledge, no electrochemical method has been reported for the determination of MMA with low detection limit to analyse the real blood sample limit. Among the electrochemical sensing, the most common traditional techniques include cyclic voltammetry (CV), differential pulse voltammetry (DPV). The major issues faced during the sensing of MMA, homo cysteine, cholesterol etc. is that they tend to undergo oxidation/reduction at the closed potentials of the conventional glassy carbon electrodes. Besides that analysis has to face lack of selectivity and reproducibility [9]. These limitations can overcome by modifying the electrodes with highly selective molecularly imprinted polymers which is having the capacity to produce notable potential difference when interacted with MMA. With the help of surface chemistry electrochemical sensing performance of an electrode can be modified. Electrode modification is the key to improve sensitivity and selectivity towards specific target molecules, which can give low detection limits of biomolecule sensing. Molecular imprinting is relatively a new and rapid evolving technique used to create synthetic receptors in polymer, recognition properties compatible to the biological system and it also possesses a great potential in several applications in life sciences [10]. This technique is used to create template shaped cavities in polymer matrices and is used for the selective and specific molecular recognition. Molecularly imprinted polymer are useful in a wide range of areas such as liquid chromatography sensing elements in sensors, artificial antibodies in immune assays, capturing matrices in solid phase extraction [11]. The polymer obtained from this technique can identify specific bioactive molecules and a sorption capacity depending on the properties and the template concentration of the surrounding medium. Thus, imprinted polymer has potential clinical, pharmaceutical and other sensing or protein adsorption applications [12]. The resulting imprinted material possesses many advantages including selectivity, sensitivity, stability, robustness, low cost. [13]. As functionalized polymers, MIPs are very suitable for fabricating electrochemical biosensors for specific recognition of targeted molecules [14,15].

GO can be easily mixed with different polymers and other materials and have attracted the interest because of its band gap and conductivity enhanced properties of composite materials such as tensile strength, elasticity, conductivity etc. GO has band gap of about 1.8 eV. Due to its unique electronic, chemical and mechanical properties, graphene oxide is used for the preparation of conducting MIP [16]. In order to enhance the conductivity of graphene oxide it is intercalated with gold nanoparticles (AuNP). AuNPs selected for the composite formation due to their optical, electronic and molecular recognition, find applications in a wide range of areas including electron microscopy, electronics, nanotechnology and material science [17]. AuNPs are incorperated into biosensors to enhance its stability, sensitivity and selectivity. It can also act as signal amplifiers, by acting as electron wire for the transport of electrons. Major types of AuNPs are based on either optical or electrochemical biosensors [18].

For the development of electrochemical sensors, silica-based materials are preferred; due to their large specific surface area, stability and three-dimensional structures made of highly open interconnected spaces. Hence, the GO/AuNP is silylated with allyl trimethoxylsilane (ATMS) resulting in a conducting polymer. This conducting polymer is used as sensitive layers in the electrochemical sensor for MMA. By introducing allylamine (AA) and 2-aminoethyl methacrylate hydrochloride (AEMA) to these polymers, functional groups of monomers of MIP could interact with MMA. In the present study, synthesis and characterization of a bulk molecularly imprinted allyl tri methoxysilane –grafted graphene oxide/gold nano particle co polymerised with -allylamine (AA)/2-aminoethyl methacrylate hydrochloride (AEMA) polymer (*GO/AuNP-g-ATMS-co-AEMA/AA)* is reported. Further, detailed electrochemical studies were performed to assess the quantitative sensing of MMA from the blood samples in selective manner.

2. Materials and methods

2.1. Reagents

Chemicals, used in the study were in the range of analytic grade. Methylmalonic acid and allyl trimethoxy silane were purchased from E. Merck India Ltd. Graphite, concentrated sulphuric acid (Con.H_2SO_4), concentrated nitric acid (Con.HNO_3), $KMnO_4$, allylamine (AA), 2-aminoethyl methacrylate (AEMA) hydrochloride, gold chloride ($AuCl_4$), dimethyl sulfoxide (DMSO) dimethyl formamide (DMF) were obtained from Alfa Aesar. Distilled water with the specific conductivity of 1μ ohm/cm was used throughout the experiments. All aqueous solutions were prepared in double distilled water. Blood samples were collected from the clinical laboratory located at Thiruvananthapuram, Kerala, India, and chilled at −4 °C before its analysis

2.2. Instruments for characterization

Cyclic voltammetry (CV) and Differential pulse voltammetry studies (DPV) were carried out by SP-200 (SN 0437), EC-Lab for windows v10.40 (software). The concentration of MMA was determined using a JASCO V-650, spectrophotometer at λmax, 263 nm. The Furrier Fourier-transform infrared spectroscopy (FTIR) spectra of the MIP were taken with Perkin Elmer 1800 model IR operating at 400–4000 cm^{-1} frequency range in transmission mode. Raman spectra were recorded with a Micro-Raman spectrometer (Lab Ram UV HR, Jobin-Yvon). XRD patterns of material were examined using Siemens D5005 X- Ray unit. Cu K∞ (λ = 1.54064 Å) radiation generated a voltage of 40 kV and current of 40 mA was used as X-ray source. Scanning electron microscopy (SEM) analyses were done using FEI model Nova Nano SEM 450 (USA) high resolution FE-scanning electron microscope. Elemental analysis was done with EDS detector, Bruker model X flash 6/10 (Germany). Atomic force microscope (AFM) images were recorded on Bruker DIMENSION Edge with SCAN ASYST instrument by taping mode. All pH measurements were carried out on a Systronics pH meter (μ pH system 362, Systronics India Ltd).

2.3. Synthesis of the electrochemical sensor (GO/AuNP-g -ATMS- co -AEMA/AA)

The synthesis of electoro chemical sensor is detailed in Scheme 1. The process involves different steps. Gold nano particles (AuNP) were synthesized through Turkevich method [19,20]. The method includes stirring of 2 ml of 0.1 M Chloro auric acid H [$AuCl_4$] s for 15 min at 80 °C in 100 ml double distilled water followed by the addition of 10 ml of 0.01 M sodium citrate. The stirring continued for 30 min keeping temperature 80 °C. Clear solution turns to vine red indicated the formation of AuNP [21,22]. GO was synthesized by modified Hummer's method [23,24]. The GO/AuNP composite was prepared by shaking 0.1 g each of GO and AuNP in a beaker containing 100 ml of deionized water for 12 h. About 0.4051 g of previously intercalated GO/AuNP was weighed and added to four necked flask, filled with 4 ml dimethyl formamide (DMF). The mixture was dispersed thoroughly by ultra-sonication for 1.5 h and about 0.4288 g of allyl trimethoxy silane (ATMS) in 40 ml DMF was added drop wise for 1 h and then stirred for 12 h at 65 °C for silylation [25]. The excess of in maintenance of nerve shea DMF in the mixture was then decanted and the residue was then washed with methanol for 2–3 times and dried in the oven. The resulting mixture is then finely powdered and stored in a storage bottle. The prepolymerization mixture was prepared by weighing about 0.5 g of MMA taken in a beaker. About 25 ml of dimethyl sulfoxide (DMSO) is added and continuously stirred for 30 min. Addition of 1 ml each of allyl amine (AA) and 2-aminoethyl methacrylate hydrochloride (AEMA) into the mixture followed by continuously stirring for 1.5 h forms the prepolymerization mixture. About 0.3240 g of SiGO/AuNP was dispersed in 25 ml of DMSO in a conical flask continue the stirring for 1.5 h.

About 0.9241 g potassium persulfate (KPS) added to the above mixture and temperature kept as at 75 °C. The pre-polymerization was then added to the above reaction mixture with continuous stirring followed by the addition of 5 ml of ethylene glycol di methacrylate (EGDMA). The resulting polymer was then washed for several times with distilled water to remove the excess DMSO and KPS. The polymer was also washed with methanol in soxhlet apparatus for 4 days and constantly till the solvent do not contain the peak of MMA at 269 nm. The polymer was dried, powdered and stored. Using the same method absolute non-imprinted polymer (GO/Au-g-ATMS-co-AEMA/AA-NIP) was prepared, without the template molecule.

2.4. Electrochemical analysis

Electrochemical work station, SP-200(SN 0437) was used for the electrochemical measurements of CV and DPV analysis. Capacity of the sensor was set at 30 ± 7 °C to keep the temperature steady during the course of measurements. Voltage window was set between −0.5 and +0.5, voltage was maintained with the range at 20 mV/s for improved operation assessment of sensor in the experimental work. Combination of 50 mM $NaClO_4$ and 5 mM [K_3Fe (CN) $_6$] was used as the supporting electrolyte. Potential for the analysis of DPV was adjusted between −0.5 and +0.5 V, pulse period 0.2 s and pulse width 0.05 s. All experiments were conducted by potential cycling in room temperature. An electrolyte solution of 50.0 mM $NaClO_4$ and 5.0 mM [$K_3Fe(CN)_6$] was used for testing [23]. The stock solution (100 μM) was diluted and added to supporting electrolyte (0.01–3.5 μM) to final concentration which is in comparable range with MMA level in human body. Analysis of low concentrations of MMA was conducted with MMA solution to check the low detection limit of the fabricated sensor.

2.5. Fabrication of imprinted sensor electrode

Molecular imprinted recognition site of glassy carbon electrode (GCE) was modified by drop cast method after polishing with abrasive paper and alumina slurry [26]. Chitosan is used as adhesive agent for stabilizing imprinted polymer on the surface of the electrode. MIP was dispersed in 0.1 M acetic acid solution containing 0.5% chitosan (CS) with ultra-sonication for 20 min. The resulting suspension (3 μL), was dropped on the cleaned GCE with MIP (GO/AuNP-co-ATMS-g-AEMA/AA) was immersed in varying concentrations of MMA solution with 25 ml supporting electrolyte at pH 7.4 for the electrochemical analysis.

2.6. Real sample analysis

The synthesized sensor was used for checking feasibility of the sensor in the real life process. Serum was separated from the blood samples. About 50 μL of aliquots of the serum were added for each analysis to the electrochemical cell of the sensor. Parameters such as linearity, analytical recovery, detection limit, sensitivity, precision and correlation were calculated using standard methods. The potential displayed by the test solutions before and after the addition of MMA were underwent the correlation study with the results obtained from a well-established diagnostic lab testing method for seventeen blood samples.

3. Results and discussion

3.1. Characterization techniques

3.1.1. FTIR analysis

The FTIR spectra of GO, $AuCl_4$, AuNP, GO/AuNP, GO/AuNP silylated, MIP polymer with MMA, MIP without MMA, Non imprinted polymer [NIP] are shown in Fig. 1. The spectrum of GO showed a broad band at 3387 cm^{-1} for –OH stretching of hydroxyl group. Band at1697 cm^{-1} indicates carbonyl stretching of –COOH group while that at

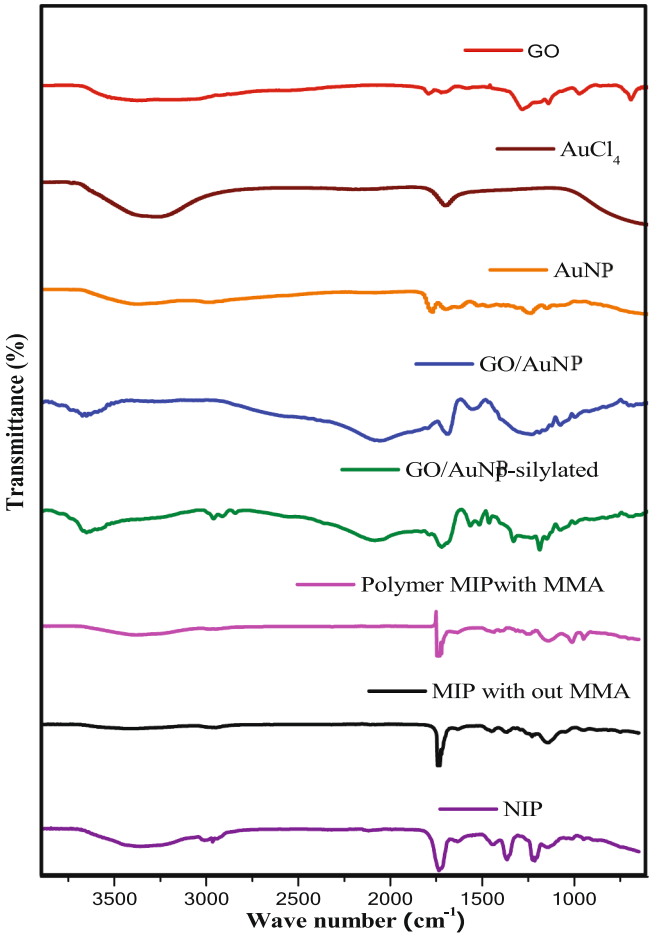

Fig. 1. FTIR spectra of Graphite, GO, $AuCl_4$, AuNP, GO/AuNP, Si- GO/AuNP, MIP-MMA, MIP, NIP.

1199 cm^{-1} specific for epoxy group onto the surface of GO. Existence of these peaks, confirms the conversion of graphite powder to GO as reported in literature [18,19]. The peak appeared at 3300 cm^{-1} of $AuCl_4$ attributes to the stretching vibration of aliphatic C–H bonds. A broad peak of AuNP around 3410 cm^{-1} indicates –OH stretching of hydroxyl group of hydrated $AuCl_4$. In the spectrum of GO/AuNP, several bands shifted and appeared at 3649, 2040, 1642, 1481 and 1180 cm^{-1}. The shifting of these bands confirm the formation of the composite GO/AuNP and the modification has been done in GO structure through the incorporation of AuNP [27]. On silylation, band intensity at 3639 cm^{-1} of hydroxyl group got reduced, indicates silyl group interacted on to the surface through oxygen containing groups from graphene surface. The peak at 2046 cm^{-1} was assigned to the stretching vibrations of methyl ($–CH_3$) and methylene ($–CH_2$) groups. The peak around 1725 cm^{-1} of MIP indicates the appearance of –COOH in the polymeric surface along with the characteristic peaks of MIP, which is the combination of Si-GO/AuNP and MMA. No characteristics bands of MMA observed in the FTIR spectrum of MIP without MMA due to the complete removal of MMA after soxhlet washing with water. This can attribute the fact that MMA is imprinted on the polymer cavity. In NIP spectrum, characteristic peaks of MIP are present which indicates chemical similarity of MIP and NIP.

3.1.2. XRD and Raman spectra analysis

The XRD patterns of graphite, GO, GO/AuNP, silylated GO/AuNP, MIP of Si-GO/AuNP without MMA, NIP of Si-GO/AuNP and MIP with MMA are shown inFig. 2. Graphite shows characteristic peak at 2θ value 23.64°. A broad peak was observed in the range of 10–11° which is reported as characteristic peak of GO [21] and this peak confirmed

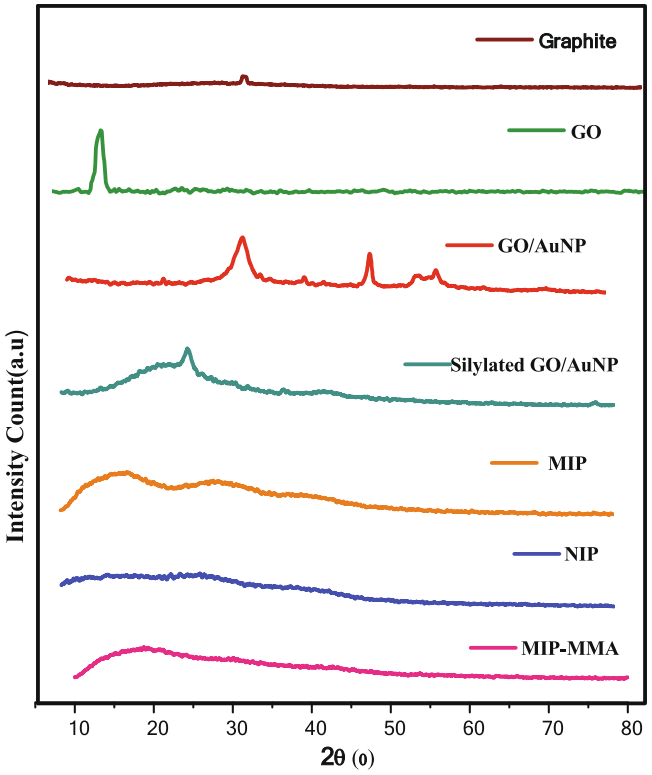

Fig. 2. XRD Patterns of Graphite, GO, GO/AuNP, Si- GO/AuNP, MIP, NIP, MIP-MMA.

the conversion of graphite to GO. Appearance of two prominent peaks at 2θ, value 26.20 and 38.08° and disappearance of characteristic GO peak in the XRD pattern of GO/AuNP indicates that the AuNP are embed inside the GO sheets. After silylation a peak of silylated GO/AuNP appeared at 2θ value 26°, the peak shift confirms the increase in the interlayer distance. Grafting of silane functionalities on the graphene sheets intercalated with AuNP gave broad peak which indicates modification has been successfully done onto the GO/AuNP surface [27]. The XRD pattern of MIP without MMA showed more amorphous spectrum which confirms the incorporation of MMA inside polymer thereby increasing polished nature of the surface. On comparing the peaks of MIP with and without MMA, a decrease in peak height observed former at 2θ values 17.9 and 17.3°. This may be due to the interaction of MMA, with the imprinting cavity of MIP surface, which make it smoother in appearance. NIP's XRD pattern is observed extremely different from that of the MIP, indicates its non-specific MMA binding site on the surface of the polymer surface.

The results of the Raman spectral analysis of graphite and GO are given in Fig. 3Fig. 3, employed to investigate micro structures of graphite and GO for confirming the conversion of graphite to GO. The prominent peaks of GO at 1360 (D band) and 1590 cm^{-1} (G band) clearly depicts the formation of GO sheets instead of multi-layer graphite. G band shows the vibration of sp^2-bonded carbon atoms while D band gives the vibration of carbon with the dangling bonds in the plane termination of graphite. The peak appeared to be symmetrical and broader which confirmed the formation of bilayer [28].

3.1.3. TEM analysis

TEM images of GO, AuNP and GO-AuNP are shown in Fig. 4. A represents the TEM image of GO showing the sheet like structure. Due to the presence of abundant functional groups and electrostatic repulsion, GO sheets are separated from each other. TEM image of AuNP clearly gave sphere like structure which substantiates the formation of AuNP from $AuCl_4$. Figure C represents the TEM image of GO/AuNP

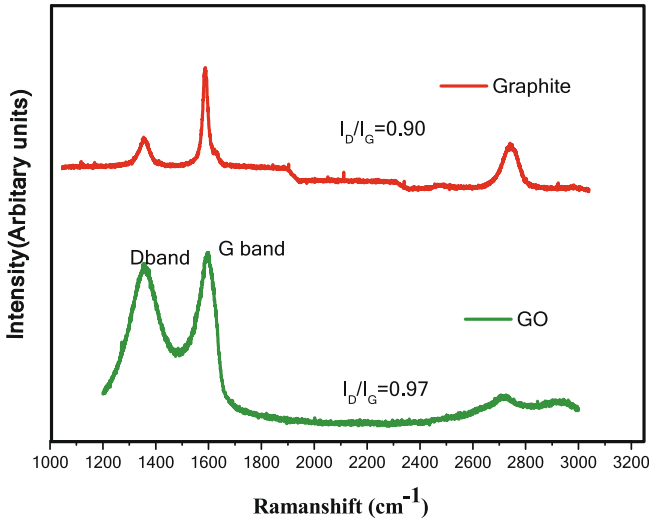

Fig. 3. Raman spectra of Graphite and GO.

which confirms the interaction of spherical AuNP in the GO sheet after intercalating the AuNP on to the GO sheets. The TEM morphology of each stage indicates the desired modification effectively done on to the GO matrix for the MIP synthesis with effective functional groups which can make remarkable H- bonding template molecule.

3.1.4. SEM analysis

SEM Images of Si GO/AuNP (A), MIP (B), MIP-MMA (C), NIP (D) are given in Fig. 5. Surface morphology of GO/AuNP confirmed the composite formation of GO with AuNP, through the appearance of spherical morphology entrapped in the GO sheets. While comparing the SEM image of MIP and MIP-MMA, the SEM image of MIP without MMA seems to be more porous than MIP-MMA, this indicates that MIP's imprinted form was successfully loaded with MMA molecules, thereby increasing the amorphous appearance on its surface. The image of MIP appears to be more porous when compared to NIP. The uniform morphology of MIP implies increased surface area through the mass transfer of templates binding on to the polymer moiety. In the SEM image of NIP, the surface was regular, more ordered and uniform as the complementary site for the recognition of MMA was not present, since specific binding sites for the recognition of MMA is absent on the surface.

3.1.5. AFM analysis

The surface morphologies of GO, AuNP, GO/AuNP, MMA-MIP and MIP are clearly depicted in AFM images given in Fig. 6. GO showed a height of around 353.2 nm in 20 μm, suggesting a single layer structure of GO [18]. The image of AuNP shows a height of about 17.7 nm. The AFM image of Si-GO/AuNP showed an increase in height of the sensor by 368.3 nm, suggesting an appreciable exfoliation has been done in GO sheets on introduction of AuNP followed by the silylation. AFM image of MIP-MMA has a peak height of only 1.1 nm, in 20 μm while the value shown by height sensor is9.6 nm for AFM image of MIP without MMA with in the same magnitude of analysis. On comparing with MIP, a decrease in height of MMA-MIP and increase in broadness could explain the successful interaction of MIP and MMA.

4. Electrochemical characterization

4.1. Cyclic voltammetry

4.1.1. Characterization of different electrodes

Electrochemical studies were conducted using the electrolytes, with the combination of electrolytes 50 mM $NaClO_4$ and 5 mM $[K_3Fe(CN)_6]$.

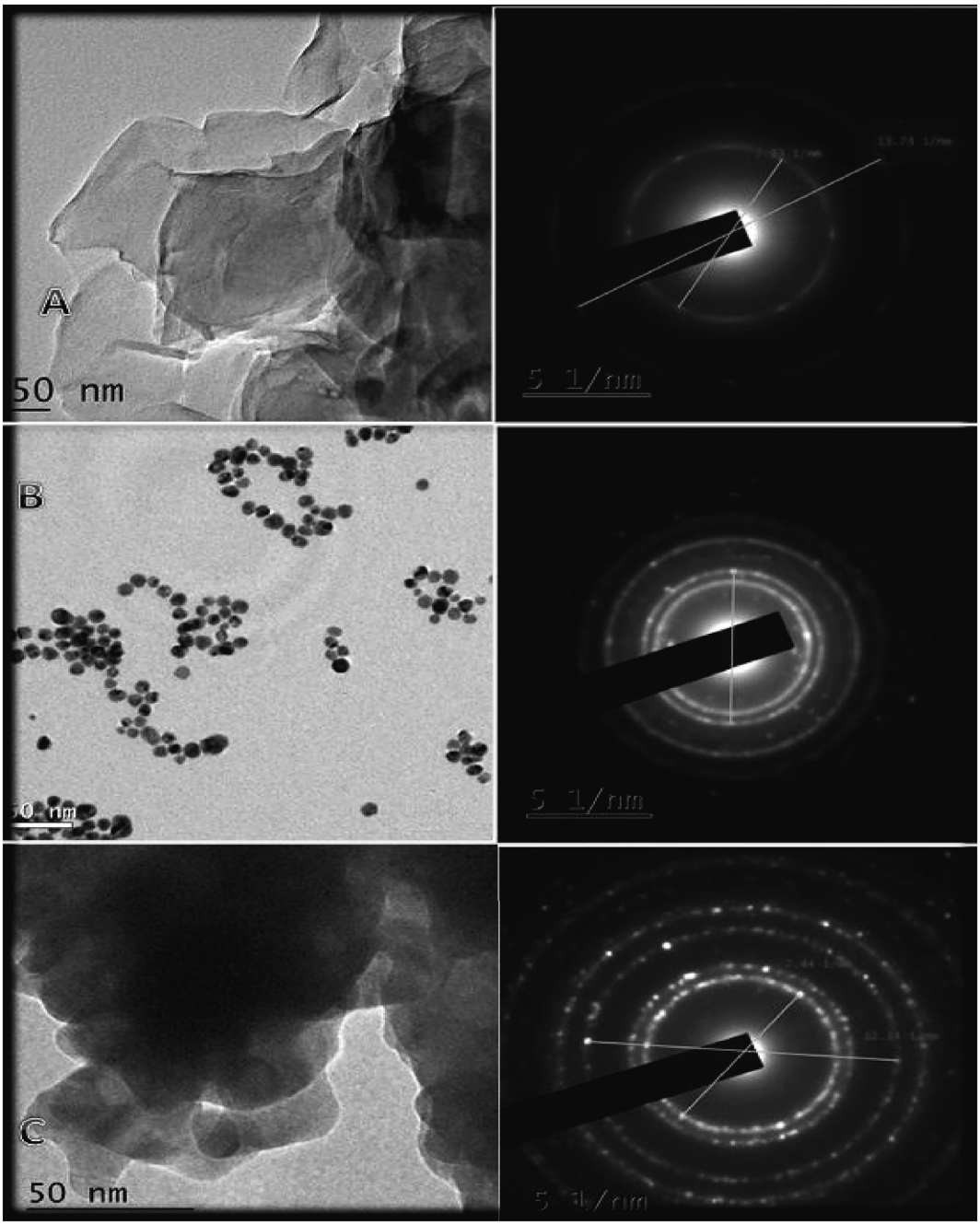

Fig. 4. TEM images of (A) GO (B) AuNP (c) GO/AuNP.

The maximum potential for bare GCE was observed to be around 0.21075 V. While the redox peak current increased to 0.1186 μA when the electrode was coated with MIP obtained for 50 mM $NaClO_4$ and 5 mM $[K_3Fe(CN)_6]$. Hence the combination concentration of chemicals in the supporting electrolyte is kept constant as 50 mM $NaClO_4$ and 5 mM $[K_3Fe(CN)_6]$. Individual experiments were carried out with 25 ml of the testing medium mixed with predominant quantity of MMA stock solution for sensor evaluation. The CV of MIP, BARE, NIP in supporting electrolyte (Fig. 7) which consists of 50 mM $NaClO_4$ and 5 mM $K_3Fe(CN)_6$, CV of $[Fe(CN)_6]^{3-/4-}$ showed a redox potential difference of 0.1109 V on the BARE GCE, whereas when the electrode is coated with MIP the redox peak current is increased to 0.1186 μA, which clearly indicates that the conductivity of MIP has increased due to the increase in the number of cavities available and thereby enhancing the conducting nature. A vacant recognition site is generated as a result of the removal of MMA from MIP allows the permeation of $[Fe(CN)_6]^{3-/4-}$ through the cavity [29,30]. Comparison of the redox current of MIP and NIP in MMA solution with supporting electrolyte is given in (Fig. 8). The peak current of MIP modified GCE is greater when compared with NIP modified GCE. Because of fewer cavity of NIP compared to MIP, the redox peak current due to NIP diminishes considerably and leads to electro insulating character over the electrode surface. The significant increase in the redox peak current indicates the excellent electrical conductivity and larger surface area of the MIP sensor electrode [31,32]. For NIP sensor, the redox peak current is greatly decreased. This might be due to the absence of electro active cavities (MIP cavities) on NIP sensor compared to MIP. A shift in potential was observed for MIP and NIP compared to bare glassy carbon is because of the conductive polymeric network. From this it could be seen that GCE with MIP modification remarkably increases the oxidation signal of MMA.

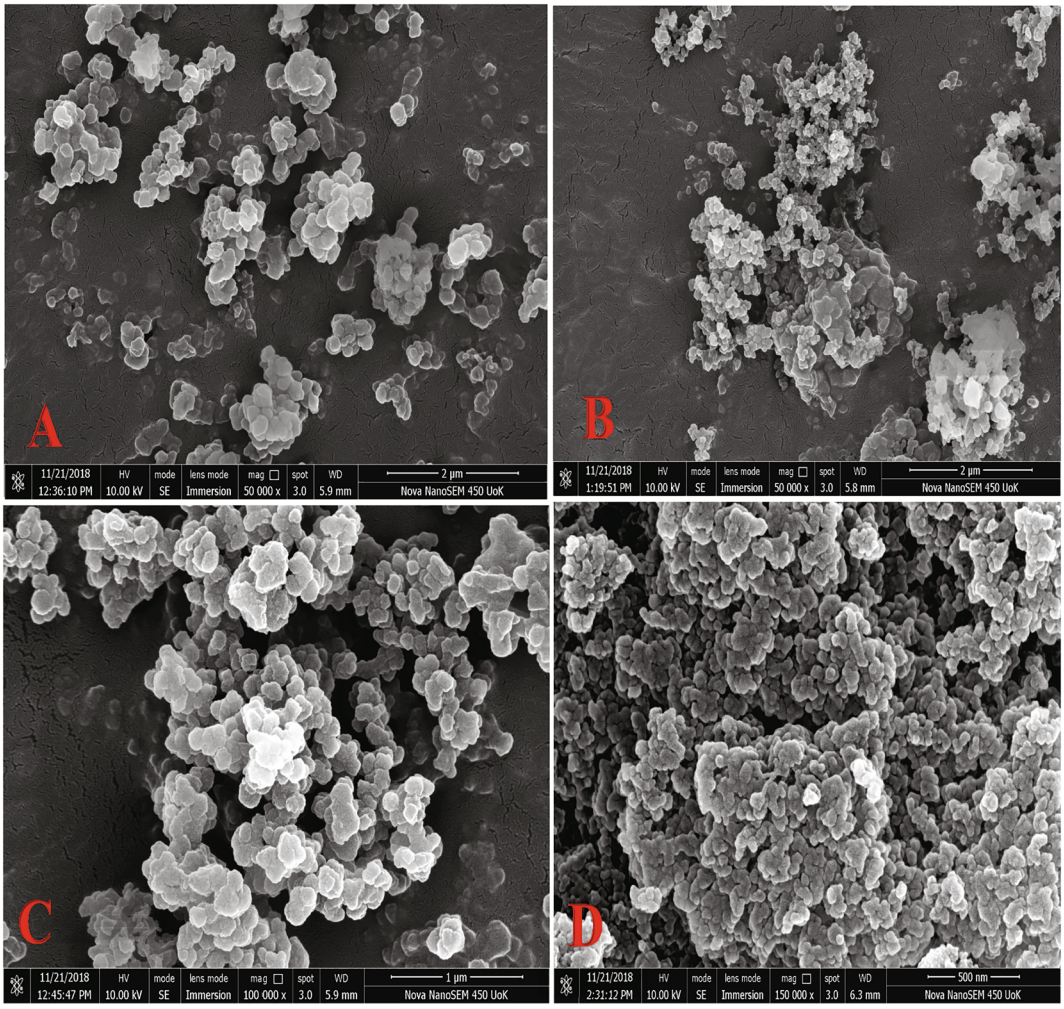

Fig. 5. SEM Images of Si GO/AuNP (A), MIP (B), MIP-MMA (C), NIP (D).

More oxidative product of MMA gets absorbed on the sensor surface, having specific site to increase the oxidation peak. MMA oxidizes through the transference of electrons towards the electrode as the concentration increases, the large oxidation wave ascribes.

4.1.2. Cyclic voltammetry analysis of different concentrations

Fig. 9 shows the electrochemical response of Si-GO/AuNP-AA-AEMA as a function of Methylmalonic acid (MMA) concentration (0.01–3.5 µM) under identical experimental conditions. Current response value increases hastily on to the addition of MMA. As the concentration of MMA increases, the redox peak current increases and may be due to the oxidation of MMA by the transference of electrons towards the electrode [27]. The CV plots indicate high sensitivity of electrode, the redox current of modified MIP- GCE in MMA is recorded as higher. This is due to the increased adsorption ability and catalytic activity for the oxidation of MMA. There could be large number of hydrogen bonding between MMA and Si-GO/AuNP-AA-AEMA, which may be the reason for improved electrochemical response for modified MMA sensor [15–17]. A graph was plotted with concentration of MMA (µM) against current (µA) indicates the linearity of the biomolecule sensing electrode with MMA concentration (0.01 – 3.5 µM). The regression coefficient (R^2) was calculated to be 0.9689 in the linear curve fit. Slope 1.643 and intercept value 33.367.

4.2. Differential pulse voltammogram (DPV) analysis

4.2.1. DPV analysis of different concentration

To investigate the response of MMA, a highly sensitive and low detection limit electrochemical method DPV was used under optimum experimental conditions. Fig. 10A depicts the typical DPV profile of MMA over difference concentration range (0.01 – 3.5 µM) using modified GCE. It was found that a well-defined and sharp oxidation peak for MMA concentration of 3.5 µM at 0.2134 V. It demonstrates the unique electrical performance and MIP promotes the electron transfer of MMA while the selective recognition site of the MIP can recognize and accumulate the MMA molecules. MIP helps to promote electron transfer to MMA which may be due to the conversion of MMA to hydroxymethoxy and pyruvic acid and oxidized through the transference of electrons towards the electrode molecule and the resultant current response was expressed [33]. A calibration graph (Fig. 10B) was also plotted with concentration against current and R^2 was found to be 0.9683. Limit of detection (LOD) was obtained from slope (K) and standard deviation (σ) by the equation:

$$LOD = 3(\sigma)/K$$

Limit of detection obtained as 0.027 µM from the slope and the standard deviation by the above equation.

Limit of quantification (LOQ) obtained as 0.92 µM using the equation:

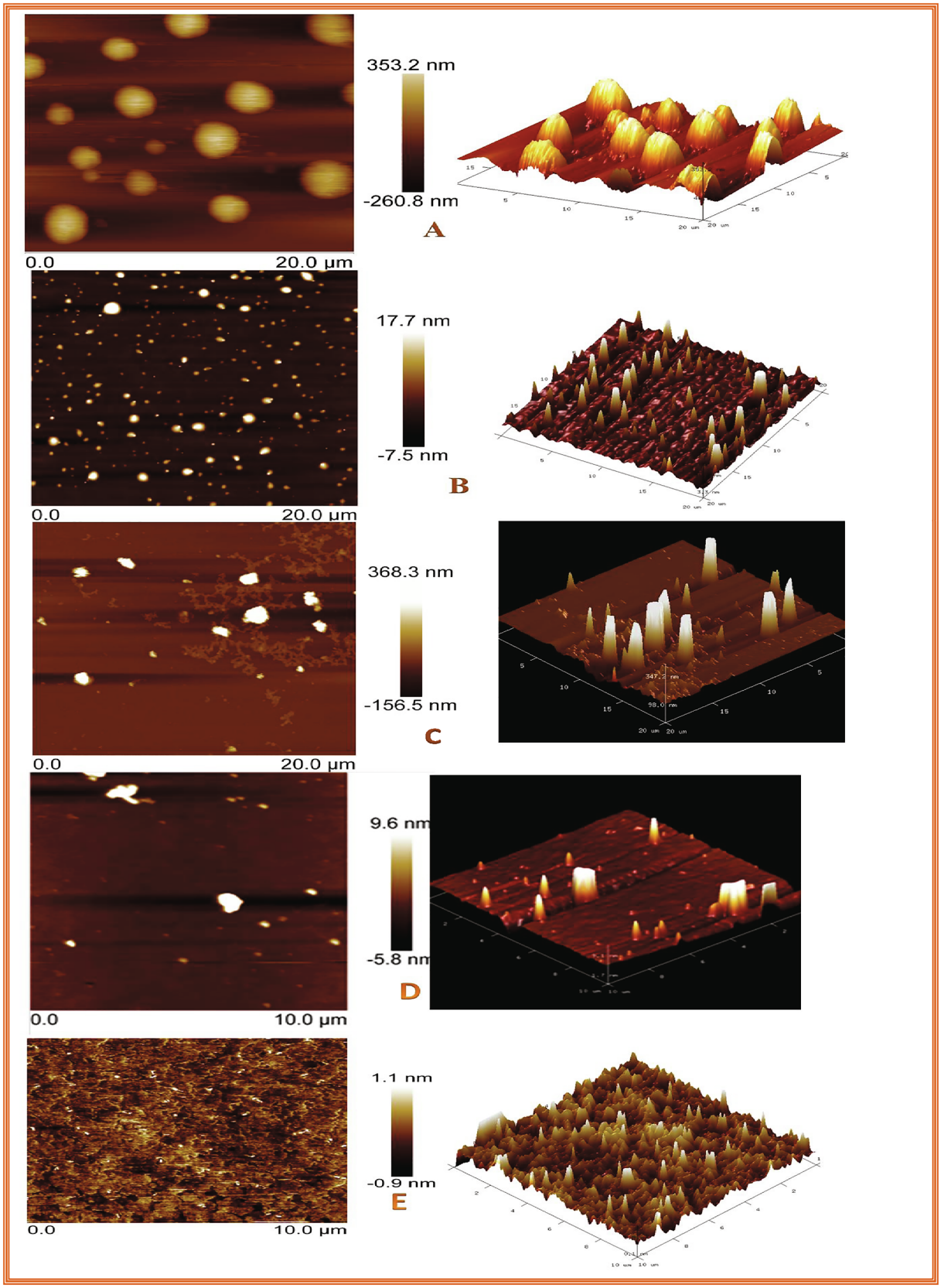

Fig. 6. AFM images of GO (A), AuNP (B), Si-GO/AuNP (C), MIP (D), and MMA-MIP (E).

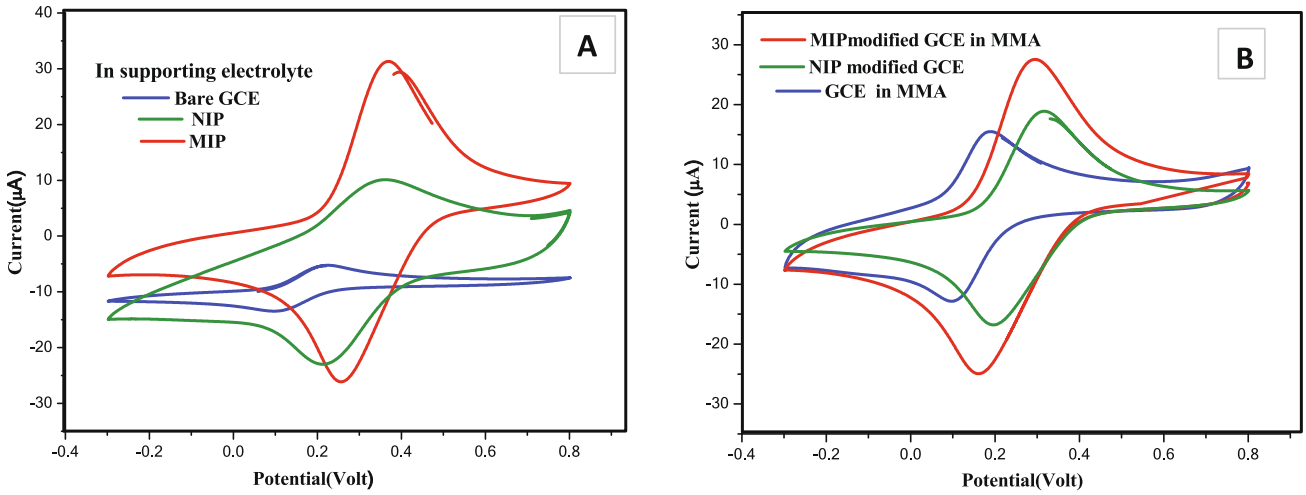

Fig. 7. A. CV response of BGC, NIP and MIP in electrolytic solution of 50 mM $NaClO_4$ and 5 mM $K_3Fe(CN)_6$;. B. Cyclic Voltammogram of Bare GCE, MIP modified GCE in MMA, NIP modified GCE.

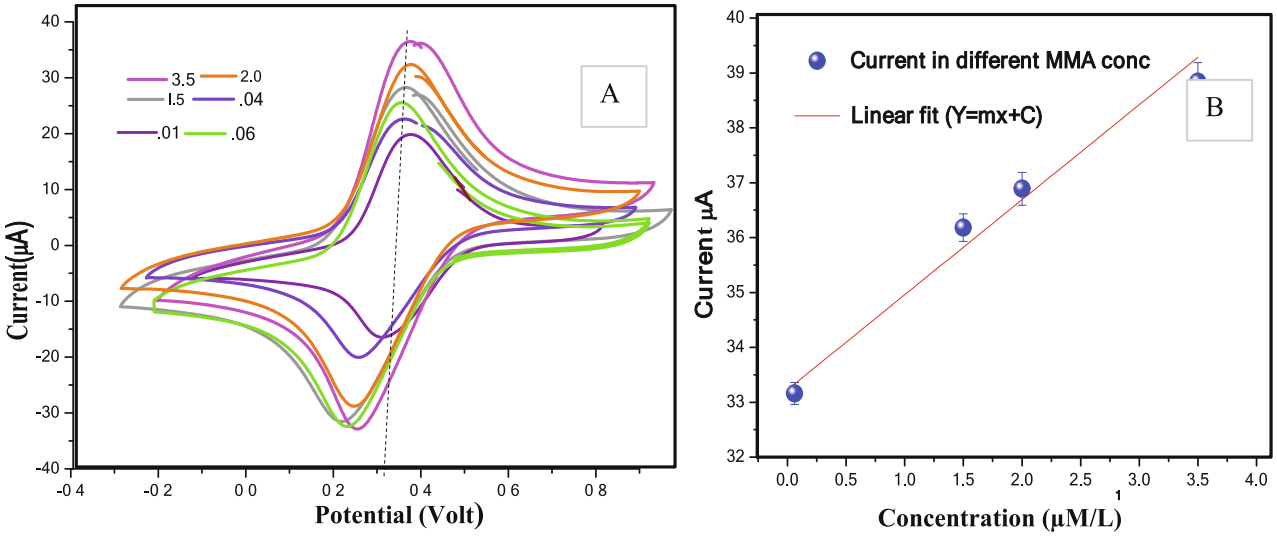

Fig. 8. Cyclic voltammogram of different MMA concentration (μM /L) solutions (A) and its concentration plot against current (μA) (B).

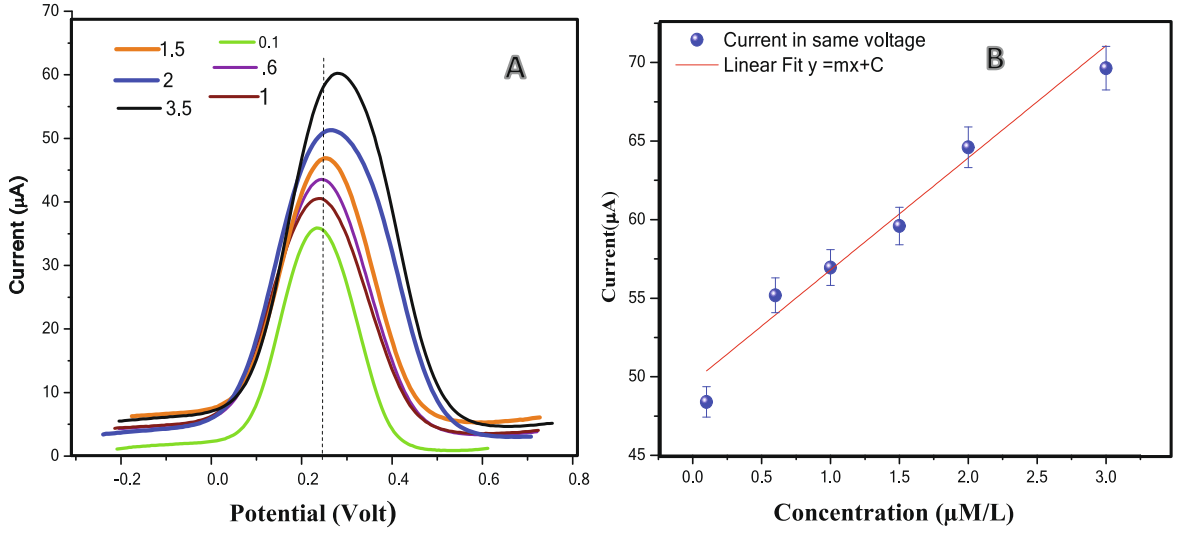

Fig. 9. DPV analysis of different MMA concentration solutions (A) and its concentration plot against current (μA) (B).

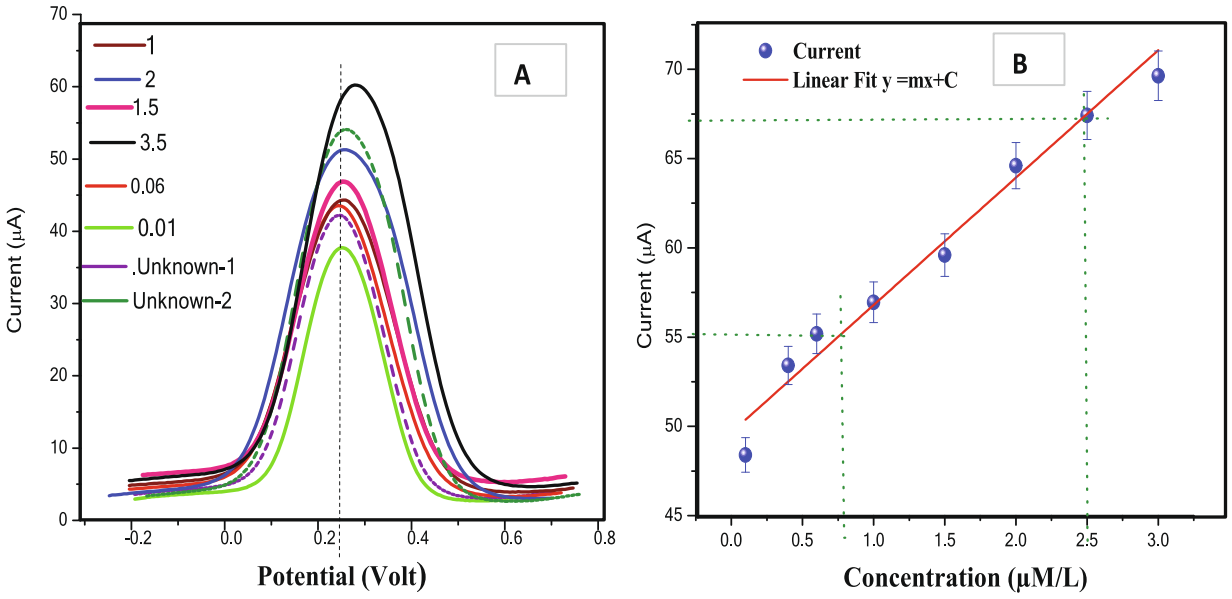

Fig. 10. DPV response of different MMA concentration solutions (A) and of unknown sample 1 and 2 and its calibration plot (B).

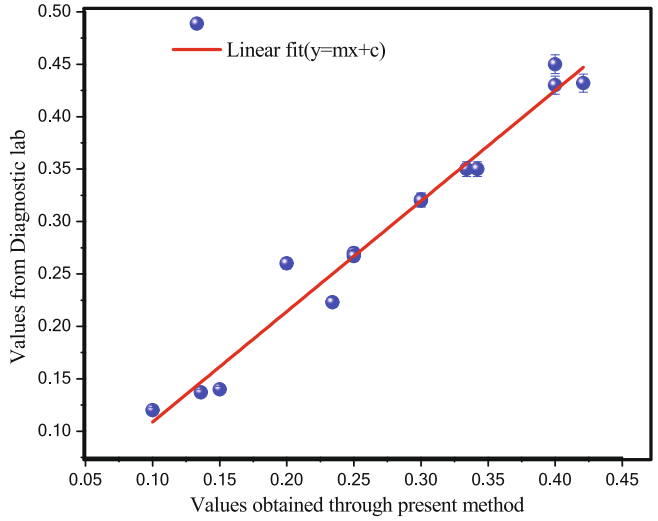

Fig. 11. Plot for the correlation of the concentration of paired clinical samples with the values of electrochemical sensor and from the traditional methodology.

$$LOQ = 10(\sigma)/K$$

4.2.2. DPV analysis of real samples

The real samples had no pre-treatment, as the MIP based sensor interacts with specific sites for MMA, which resides on the surface of MIP. The blood serum samples were analysed using Si-GO-MMA-AA-AEMA coated GCE and the current responses for the samples were noted, using the calibration plot and the corresponding concentrations were obtained. To check the performance of the sensor for routine analysis, the sensor was applied to determine MMA in blood serum samples [34]. No pre-treatment on the sample, since the MIP based sensor could bind some non-specific molecules from the real samples. DPV diagrams for different concentrations of MMA solution with which MIP modified GCE and current versus MMA concentration calibration plots are shown in Fig. 10A. Linearity check of the analysis is carried out and good linearity with the observed reading with regression coefficient 0.963 is obtained and is given in Fig. 10.B. The unknown concentration of MMA in the collected blood samples was checked with DPV analysis and from the plot of current against concentration (Fig. 11.A & .B). The MMA content corresponds to 55.501 μA and 67.2 μA in unknown sample 1 and unknown sample 2 are 0.6 and

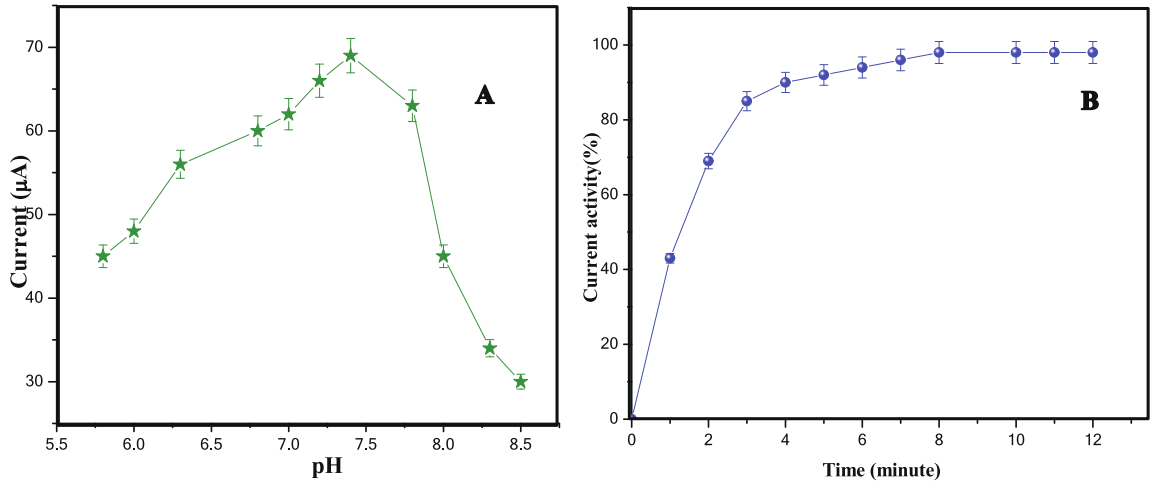

Fig. 12. Plot of Current Vs pH variation of 3.5 μM/LMMA solution (A), Current (%) Vs time plot of 3.5 μM/LMMA solution (B).

Table 1
Comparison of the MMA sensor with HPLC method.

Concentration (μmol/L)	HPLC	R.S.D (%)	DPV	R.S.D (%)
5.00	4.60	0.462	4.860	0.356
10.0	9.10	0. 634	9.343	0.515
15.0	14.10	0.623	14.63	0.234

2.5 μM/L, respectively. These observed values show good agreement with the results collected from the measured in Das Medical Diagnostic Centre, Medical College Road, Thiruvananthapuram, Kerala, India using HP GC/MSD method; thereby indicating that the Si-GO-MMAAA-AEMA (MIP) sensor is feasible in the routine analysis of MMA from the blood samples. Several clinical samples were checked for MMA concentration by both methods. A comprehensive comparison was also made between the MIP sensor and clinical examination results. In order to check the reliability and proximity of the values by the current method 15 clinical samples were cross-checked with a diagnostic laboratory methodology. A linear correlation plot (Fig. 12) gave a better regression coefficient 0.9678 indicates the synthesized sensor possessing a comparable sensitivity with the practicing MMA checking method in the diagnostic lab. Electro chemical sensor required only 20 μL of blood sample. The MIP based sensor had very comparable results with the results obtained from clinical examination. With the help the slope of the line and standard deviation using the above equation (1) Limit of detection obtained as 0.2095 μM/L. Limit of quantification (LOQ) was obtained as 0.2935 Mm using the Eq. (2)

4.3. Comparison of the MMA sensor with HPLC method.

The different techniques feasible for the analysis employed to check the concentration of MMA. Values obtained on the HPLC technique and present methods compared and are listed in the Table 1. Found more accurate with low RSD values in the present method compared to other values indicates the effectiveness of fabricated sensor[35].

4.4. Reproducibility stability and repeatability of modified GCE with GO/AuNP-g-ATMS-co-AEMA/AA

The reproducibility and repeatability of values in the electrochemical sensing of MMA with modified GCE by *GO/AuNP-g-ATMS-co-AEMA/AA* monolayers were performed with three different concentrations 1, 5 and 10 μM of solution in triplicate manner. Reproducibility of values on different set of experiments were done after an interval, of time in the same experimental conditions and the results are tabulated in S.1. After each analysis dipping the modified GCE in ethanol and washing it thoroughly with water for 12 h and dried in vacuum after each electrochemical measurement. The sensor could be reused after cleaning process without loss in performance in the sensing of MMA even after different sets of experiments and the lower value of RSD in different sets of experiment clarified the stability of fabricated sensor is relatively good. The repeatability of the sensor fabricated also checked using same concentrations 1, 5 and 10 μmol/L solutions of MMA with three different sensors. GCE polished with abrasive paper and alumina slurry after each analysis and further analysis was done with new MIP drop casted the GCE to fabricate sensing membrane. Values of the current obtained for each experiment is closely related with low RSD value [36,37]. The testing results and relative standard deviations are shown in S.2. From these experimental results and appreciable RSD values confirm the repeatability of the sensor could be acceptable for practical purposes.

4.5. Effect of solution incubation time and solution pH

Fig. 12.A represents effect of incubation on the redox potential of

Table 2
Comparison of efficiency of GO/AuNP-g-ATMS-co-AEMA/AA, electro chemical sensor with other reported methods.

No	technique	Detection limit	Comments	Reference
1	Isotope-dilution gas chromatography–Mass spectrometry (gc-ms) method	0.03 μM/L	The GC–MS analysis is characterized by selectivity, sufficient sensitivity, and good precision, withCVs often ⩽3%	[37]
2	HPLC combined with liquid chromatography electrospray ionization tandem mass spectrometry (LC-ESI-MS/MS).	0.1 μM/L (signal-to-noise ratio > or = 10).	simple and reliable high-throughput method for the determination of MMA that is suitable for automation.	[38]
3	Liquid chromatography (LC)-MS/MS system using TurboIonSpray (nebulizer-assisted electrospray) ionization and quantified by the multiple reaction monitoring mode of MS/MS.	0.05 μM/L	The LC–MS/MS analysis for MMA requires minimal chromatographic separation and takes < 60 s per sample	[39]
4	liquid chromatography tandem mass spectrometry (LC-MS/MS)	0.1 μM/L	Using solid phase extraction for sample preparation	[40]
5	Eectrochemical sensing	0.2095 μM/L	Voltammetric sensor utilizes a work voltage at 50 mV/s for analysis. Linear range of 0.5–3 mg/dL is satisfactory for detection of high Cn levels	[Present work]

$K_3[Fe(CN)_6]$ with MMA solution studied with in time range 1–15 min. The optimum response time was found to be 8 min with a standard deviation not exceeding 3.0%. The effect of solution pH was optimized (Fig. 12.B.) by a series of phosphate buffer in the range 2.0–8.0 and the optimum response obtained was at pH 7.4 which is compared to pH of blood, this could substantiate suitability in analysis of MMA concentration in blood with fabricated sensor.

4.6. Comparison of efficiency of GO/AuNP-g-ATMS-co-AEMA/AA, electro chemical sensor

A comprehensive comparison was made between the GO/AuNP-g-ATMS-co-AEMA/AA sensor and the recently reported various methods and technique [37–40] for determination of MMA (Table 2). The results indicated that the MIP based GO/AuNP-g-ATMS-co-AEMA/AA provided wide linear range and low detection limit for the electrochemical sensing of MMA. It should be noted that there voltammetry sensor utilizes a work voltage is maintained within the range at 50 mV/s for analysis. Linear range of 0.5–3.0 mg/dL is satisfactory for detection of high MMA levels, with in the range of MMA level in the blood serum.

5. Conclusions

An electrochemical sensor for the determination of MMA in human blood has been developed as there is lack of direct method for the determination of VB-12 imbalance, in the blood. The profits the inherent properties of GO, AuNP, AEMA and AA constitute a matrix suitable for the arrest of MMA though the H- bonding stabilization with the molecularly imprinted site. When MMA captured by the membrane, it develops a closer proximity between the MMA and the sensor and could results faster and accurate response. The constructed sensor exhibits great selectivity and its usefulness for the rapid determination of MMA in human serum. The advantages of the designed electrode are its reproducibility, long lasting and no pre-treatment of biological samples required during clinical analysis. These results could support reliability of the sensing system based on MIP for real life analysis. Furthermore a comprehensive comparison was made between the MIP sensor and the clinical examination results. Concentration of MMA obtained from the present method was paired with15 clinical samples using HP GC/MSD method both the values gave good linear correlation with regression coefficient value 0.967. The values obtained in all the electrochemical studies could confirm the strong candidature of fabricated sensor in the field of analysis of MMA.

Declaration of Competing Interest

T. S. Anirudhan and co-authors (Dr. J. R. Deepa, Gowri Soman and V. Chithra Sekhar) declare that we have no conflict of interest (financial or non-financial) and hence request you to kindly consider our research paper cited above for review process.

Acknowledgments

The authors are thankful to Professor and Head, Department of Chemistry, School of Physical and Mathematical science, University of Kerala, Trivandrum, India for providing the laboratory facilities. One of the authors, Dr. J. R. Deepa is grateful to DST–PURSE programme University of Kerala, Trivandrum, for the Post-Doctoral fellowship for this work.

Appendix A. Supplementary data

Supplementary data to this article can be found online at https://doi.org/10.1016/j.microc.2020.105489.

References

[1] M.S. Carol, K. George, Summer, gas-chromatographic determination of methylmalonic acid in urine and serum, Clin. Chem. 20 (1974) 444–446.
[2] H.S. Theresa, T.A.W. Quay, L. Yvonne, Methylmalonic acid quantified in dried blood spots provides a precise, valid, and stable measure of functional VitaminB-12 status in healthy women, J. Nutr. 144 (2014) 1658–1663.
[3] A.M. Molloy, P.N. Kirke, J.F. Troendle, H. Burke, M. Sutton, L.C. Brody, J.M. Scott, J.L. Mills, Maternal VitaminB-12 status and risk of neural tube defects in a population with high neural tube defect prevalence and no folic acid fortification, Pediatrics 123 (2009) 917–923.
[4] R. Clarke, P. Sherliker, H. Hin, E. Nexo, A.M. Hvas, J. Schneede, J. Birks, P.M. Ueland, K. Emmens, J.M. Scott, Detection of Vitamin B-12deficiency in older people by measuring Vitamin B-12 or the active fraction of Vitamin B-12. holo trans cobalamin, Clin. Chem. 53 (2007) 963–970.
[5] C. Hempen, H. Wanschers, G. van der Sluijs Veer, A fast liquid chromate graphic tandem mass spectrometric method for the simultaneous determination of total Homocysteine and methyl malonic acid, Anal. Bioanal. Chem. 391 (2008) 263–270.
[6] A.J. MacFarlane, L.S. Greene-Finestone, Y. Shi Y, VitaminB-12 and homocysteine status in a folate-replete population: results from the Canadian Health Measures Survey, Am. J. Clin. Nutr. 94 (2011) 1079–1087.
[7] K. Bjorkegren, K. Svardsudd, Elevated serum levels of methylmalonic acid and homocysteine in elderly people. A population-based intervention study, J. Internal Medi. 246 (1999) 317–324.
[8] E.A. Yetley, C.M. Pfeiffer, K.M. Phinney, R.L. Bailey, S. Blackmore, J.L. Bock, L.C. Brody, R. Carmel, L.R. Curtin, R.A. Durazo-Arvizu, et al., Biomarkers of Vitamin B-12 status in NHANES: a roundtable summary, Am. J. Clin. Nutr. 94 (2011) 313S–21S.
[9] H. Dong, W. Gao, F. Yan, H. Ji, H. Ju, Fluorescence and resonance energy transfer between quantum dots and graphene oxide or sensing bio molecules, Anal. Chem. 82 (2010) 5511–5517.
[10] T.S. Anirudhan, J.R. Deepa, A.S. Nair, Fabrication of chemically modified graphene oxide/nano hydroxyapatite composite for adsorption and subsequent photocatalytic degradation of aureomycine hydrochloride, J. Ind. Eng. Chem. 47 (2017) 415–430.
[11] R. Gui, H. Jin, H. Guo, Z. Wang, Recent advances and future prospects in molecularly imprinted polymers-based electrochemical biosensors, Biosen. Bioelectr. 100 (2018) 56–70.
[12] R. Gui, H. Guo, H. Jin, Preparation and applications of electrochemical chemosensors based on carbon-nanomaterial-modified molecularly imprinted polymers, Nano Adv. 1 (2019) 3325–3363.
[13] H. Guo, R. Gui, H. Jin, Z. Wang, Facile construction of reduced graphene oxide–carbon dot complex embedded molecularly imprinted polymers for dual-amplification and selective electrochemical sensing of rutoside, New J. Chem. 41 (2017) 9977–9983.
[14] H. Jin, H. Guo, X. Gao, R. Gui, Selective and sensitive electrochemical sensing of gastrodin based on nickel foam modified with reduced graphene oxide/silver nanoparticles complex-encapsulated molecularly imprinted polymers, Sens. Actuators B Chem. 277 (2018) 14–21.
[15] S.H. Kang, T.H. Fang, Z.H. Hong, Electrical and mechanical properties of graphene oxide on flexible substrate, J. Phys. Chem. Solids 74 (2013) 1783–1793.
[16] T.S. Anirudhan, J.R. Deepa, Binusreejayan, Electrochemical sensing of cholesterol by molecularly imprinted polymer of silylated graphene oxide and chemically modified nanocellulose polymer, Mater. Sci. Eng. C 92 (2018) 942–956.
[17] T.S. Anirudhan, J.R. Deepa, S. Nisha, Fabrication of a molecularly imprinted silylated graphene oxide polymer for sensing and quantification of creatinine in blood and urine samples, Appl. Surf. Sci. 466 (2019) 28–39.
[18] S.A. Zaidi, Molecular imprinting polymers and their composites: a promising material for diverse applications, Biomater. Sci. 3 (2017) 388–402.
[19] T.S. Anirudhan, J.R. Deepa, Nano-zinc oxide incorporated graphene oxide/nanocellulose composite for the adsorption and photo catalytic degradation of ciprofloxacin hydrochloride from aqueous solutions, J. Colloid Interface Sci. 490 (2017) 343–435.
[20] N.I. Zaaba, K.L. Foo, U. Hashim, S.J. Tan, W.W. Liu, C.H. Voon, Synthesis of graphene oxide using modified hummers method: solvent influence, Proc. Eng. 184 (2017) 469–477.
[21] Y.C. Yeh, B. Creran, V.M. Rotello, Gold nanoparticles: preparation, properties, and applications in bionanlytical technology, Nanosci. 4 (2012) 1871–1880.
[22] Z. Jingyue, F. Bernd, Synthesis of gold nanoparticles via chemical reduction methods. Nanocon. 597–604. DOI:10.13140.
[23] T.S. Anirudhan, J.R. Deepa, Binusreejayan, Synthesis and characterization of multi-carboxyl-functionalized nanocellulose/nanobentonite composite for the adsorption of uranium (VI) from aqueous solutions: kinetic and equilibrium profiles, Chem. Eng. J. 273 (2015) 390–400.
[24] N. Elgrishi, K.J. Rountree, B.D. McCarthy, E.S. Rountree, T.T. Eisenhart, J.L. Dempsey, A practical beginner's guide to cyclic voltammetry, J. Chem. Edn. 95 (2018) 197–206.
[25] J. Kimling, M. Maier, B. Okenve, V. Kotaidis, H. Ballot, A. Plech, Turkevich method for gold nanoparticle synthesis revisited, J. Phy. Chem. B 110 (2006) 15700–15707.
[26] T. Rattana, S. Chaiyakun, N. Witit-Anun, N. Nuntawong, P. Chindaudom, S. Oaew, P. Limsuwan, Preparation and characterization of graphene oxide nanosheets, Procedia Eng. 32 (2012) 759–764.
[27] A. Kaniyoor, S.A. Ramaprabhu, Raman spectroscopic investigation of graphite oxide derived graphene, AIP Adv. 2 (2012) 0–13.
[28] J.N. Tiwari, V. Vij, K.C. Kemp, K.S. Kim, Engineered carbon-nanomaterialbased electrochemical sensors for biomolecules, ACS Nano 10 (2016) 46–80.

[29] M. Pumera, A. Ambrosi, A. Bonanni, E.L.K. Chng, H.L. Poh, Graphene for electrochemical sensing and biosensing, TrAC - Trend Anal. Chem. 29 (2010) 954–965, https://doi.org/10.1016/j.trac.2010.05.011.
[30] A.L. Joke Chow, S.A. Bhawani, Synthesis and characterization of molecular imprinting polymer microspheres of cinnamic acid: extraction of cinnamic acid from spiked blood plasma, Int. J. Polym. Sci. 2 (2016) 1–5.
[31] S.K. Sharma, N. Sehgal, A. Kumar, Biomolecules for development of biosensors and their applications, Curr. Appl. Phys. 3 (2003) 307–316.
[32] C. Xue, Q. Han, Y. Wang, J. Wu, T. Wen, R. Wang, H. Jiang, Amperometric detection of dopamine in human serum by electrochemical sensor based on gold nanoparticles doped molecularly imprinted polymers, Biosens. Bioelectron 49 (2013) 199–203.
[33] P. Mehrotra, Biosensors and their applications - a review, J. Oral Biol. Cranio. Fac. Res. 6 (2016) 153–159.
[34] A. Sacco, Electrochemical impedance spectroscopy: fundamentals and application in dye-sensitized solar cells, Renew. Sustain. Energy Rev. 79 (2017) 814–829.
[35] T.S. Anirudhan, V.S. Athira, V.C. Sekhar, Electrochemical sensing and nano molar level detection of Bisphenol-A with molecularly imprinted polymer tailored on multiwalled carbon nanotubes, Polymer 146 (2018) 312–320.
[36] F. Li, X. Jiang, J. Zhao, S. Zhang, Graphene oxide: a promising nanomaterial for energy and environmental applications, Nano Energy 16 (2015) 488–515.
[37] W. Amrei, A. Ove, K. Gry, U. Per Magne, Automated assay for the determination of methylmalonic acid, total homocysteine, and related amino acids in human serum or plasma by means of methyl chloro formate derivatization and gas chromatography–mass spectrometry, Clin. Chem. 51 (2005) 12103–12109.
[38] J.B. Henk, R. Arno van, H. Marije, A simple high-throughput method for the determination of plasma methylmalonic acid by liquid chromatography-tandem mass spectrometry, Clin. Chem. Lab. Med. 45 (2007) 645–650.
[39] M.M. Kushnir, G. Komaromy-Hiller, B. Shushan, F.M. Urry, W.L. Roberts, Analysis of dicarboxylic acids by tandem mass spectrometry. High-throughput quantitative measurement of methylmalonic acid in serum, plasma, and urine, Clin. Chem. 47 (2001) 1993–2002.
[40] A. Gallego-Narbón, Z. Belen, A. Inmaculada, M.P. Vaquero, Methylmalonic acid levels and their relation with cobalamin supplementation in spanish vegetaria, Plant Food Hum. Nutr. 73 (2018) 166–171.